A Localized and Packetized Approach to Distributed Power Inverter Management

Luis A. Duffaut Espinosa and Jeff Frolik
Department of Electrical and Biomedical Engineering
University of Vermont, Burlington, VT 05405

***Abstract*—Local management of solar photovoltaic and battery inverters is seen as a means to mitigate many grid issues that can result from large penetrations of distributed and variable solar energy. This work demonstrates through simulation how local inverter operation can fit within an operational paradigm referred to as packetized energy management. In particular, the power factor at which energy packets are injected in to the grid from a distributed set of energy resources (i.e., batteries) are adjusted in discrete steps over the range of operation. Unlike approaches where a device's power factor is adapted continuously over time, the discrete-time and asynchronous nature of the investigated approach avoids potential system oscillations. We present simulation results for a feeder line consisting of 100 battery systems comparing our distributed, locally-controlled approach to one centrally determined and controlled.**

***Index Terms*—Packetized energy management, power inverters, power factor.**

I. Introduction

The coordination of distributed energy resources (DERs) to help manage grid dynamics is seen no longer as a promising technology but as requisite in order to achieve an 100% renewable electric grid, protect aging infrastructure, etc. [1]. Inverter-based DERs (e.g., distributed solar, battery storage, and vehicle-to-grid (V2G) electric cars) can not only inject power into the grid, but also inject it at non-unity power factors based on the grid's needs for voltage/frequency regulation. The work herein presents a localized approach for inverters to autonomously adjust power factors based on local information. While this idea is not new [2], [3], the approach considered in this work is the first that leverages a DER coordination approach known as packetized energy management (PEM) [4].

In contrast to the top-down DER management approaches, under PEM, DERs request energy transfer (as a load and/or as a source) based on their real-time needs and the aggregator that is managing the DER fleet accepts/denies these requests based on real-time grid/market conditions. The approach leverages two key concepts from data communications that enable billions of devices to operate across the Internet: *packetization* and *randomization*. When a device, such as a residential battery, requests energy, it is only for a fixed and finite period of time (e.g., 5 minutes). This is akin to breaking a large data file into fixed length data packets. Under PEM, each battery requests either to receive (i.e., charge) or provide (i.e., discharge) a packet with a probability that depends on its current *state of charge*, SOC. Each request is treated independently by the system aggregator. One battery system's actions occur independently according to simple rules. Furthemore, actions of one battery occurs asynchronously of the other batteries in the system; this asynchronicity mitigates the potential for system oscillation as we will show in this work.

KEY contributions of this paper are as follows.

This work was supported by a National Science Foundation STTR Phase I award (IIP-1722008) and a U.S. Department of Energys Advanced Research Projects Agency - Energy (ARPA-E) grant (DE-AR0000694).

J. Frolik is among the co-founders of Packetized Energy Technologies, Inc, which seeks to bring to market a commercially viable version of packetized energy management.

1) We present underlying local rules by which a battery inverter will adjust its power factor.
2) Our localized approach for inverter power factor management is compared to a centrally determined approach.
3) We provide a simple bound for voltage deviation at each node by characterizing the steady state probabilities using a three state Markov chain obtained from the underlying PEM mechanics.

II. Preliminaries and Methods

This section provides the basic background for PEM and the characterization of the inverters acting as the interface between ESSs and a simplified linear grid.

A. Packetized energy management fundamentals

The following three statements summarize the key idea behind PEM [4]:

i. A DER measures its local dynamic state (e.g., energy level, SOC).
ii. If the state exceeds locally defined limits, the DER exits PEM, reverts to a default DER control mode until the state is returned to within limits and returns to Step 1. Else, based on the state, the DER probabilistically requests to consume (inject) energy at a fixed rate from (into) the grid for a pre-specified period of time (i.e, an *energy packet*).
iii. The coordinator (or *Virtual Power Plant*, VPP) either accepts or denies the DER's packet request based on grid or market conditions, such as power reference tracking error or grid capacity constraints. If a request is denied, then the logic returns to Step 1. In the case of the request being accepted, the DER consumes or injects energy for the duration of the packet and then returns automatically to Step 1.

PEM ensures quality of service (QoS) by utilizing a probabilistic request rule based on the local dynamic state of each DER. In addition, if QoS falls behind certain pre-defined threshold, then DERs are capable of exiting PEM. Synchronization is avoided by introducing randomization to the DER's requests with respect to the local state variables (e.g., ESS requests are made with probability dependent on their corresponding SOC). The typical closed loop block diagram of a PEM system is shown in Fig. 1.

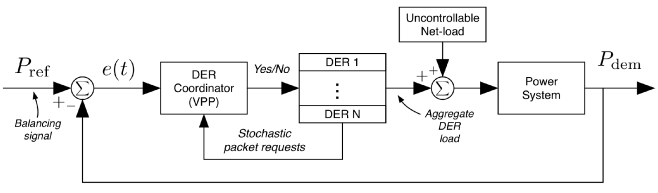

Fig. 1. Closed-loop feedback system for PEM with $P_{\text{ref}}(t)$ provided by the grid or market operator and the aggregate net-load $P_{\text{dem}}(t)$ measured by VPP.

Let the energy state of the n-th DER in a fleet be denoted as z_n. The equation for this DER is written as the following discrete-time dynamic model

$$z_n^+ = f_n(z_n, \phi_n, P_{\mathrm{c},n}^{\mathrm{rate}}, P_{\mathrm{d},n}^{\mathrm{rate}}, w_n), \tag{1}$$

where f_n is some one-dimensional nonlinear mapping (usually linear or bilinear), w_n is the parameter mapping end-consumer usage to the energy state, $P_{\mathrm{c},n}^{\mathrm{rate}}$ and $P_{\mathrm{d},n}^{\mathrm{rate}}$ are the energy transfer rates of the n-th DER when charging (c) or discharging (d), respectively, and ϕ_n is the hybrid state corresponding to the set of modes $\{\mathrm{c}, \mathrm{sb}, \mathrm{d}\}$ associated to $\{$charge, standby, discharge$\}$, respectively [4], [5]. In this manuscript, the focus is put on bidirectional energy storage systems (ESSs); i.e., batteries such as the residential systems provided by Enphase, LG and Tesla. Equation (1) for an ESS with background power usage w_n and $P_{\mathrm{c},n}^{\mathrm{rate}}, P_{\mathrm{d},n}^{\mathrm{rate}} > 0$ is

$$z_n^+ = \eta_{\mathrm{sl},n} z_n + \phi_n u_{\phi_n,n} \eta_{\phi_n,n} + w_n, \tag{2}$$

where $u_{\phi_n,n}$ is $P_{\mathrm{c,n}}^{\mathrm{rate}}$ for $\phi_n = \mathrm{c}$, $P_{\mathrm{d,n}}^{\mathrm{rate}}$ for $\phi_n = \mathrm{d}$ and 0 for $\phi_n = \mathrm{sb}$ in [kW], and $\eta_{\mathrm{sl},n}$, $\eta_{\mathrm{c},n}$, and $\eta_{\mathrm{d},n}$ are the standing losses, charging, and discharging parameters, respectively. Herein, an ESS is modeled as a bidirectional battery in which simultaneous charging and discharging are not permitted. The probability of requesting an energy packet for the n-th DER with dynamic state $z_n[k] \in [\underline{z}_n, \overline{z}_n]$ and desired set-point $z_n^{\mathrm{set}} \in (\underline{z}_n, \overline{z}_n)$ at time k (for discretization time-step Δt) is given by

$$P(z_n[k]) := 1 - e^{-\mu(z_n[k])\Delta t}, \tag{3}$$

where $\mu(z_n[k]) > 0$ is a rate parameter dependent on the local dynamic state. The dependence on the local dynamic state for the request probability is established by considering the boundary conditions:

$$i. \quad P_k^{\mathrm{c}}(n | z_n[k] \le \underline{z}_n) = 1, \quad P_k^{\mathrm{c}}(n | z_n[k] \ge \overline{z}_n) = 0,$$

$$ii. \quad P_k^{\mathrm{d}}(n | z_n[k] \le \underline{z}_n) = 0, \quad P_k^{\mathrm{d}}(n | z_n[k] \ge \overline{z}_n) = 1,$$

from which $i.$ gives rise to the following helpful design of $\mu(z_n[k])$ for *consuming* a packet:

$$\mu(z_n[k]) = \begin{cases} 0, & \text{if } z_n[k] \ge \overline{z}_n \\ m_R \left(\frac{\overline{z}_n - z_n[k]}{z_n[k] - \underline{z}_n} \right) \cdot \left(\frac{z_n^{\mathrm{set}} - \underline{z}_n}{\overline{z}_n - z_n^{\mathrm{set}}} \right), & \text{if } z_n[k] \in (\underline{z}_n, \overline{z}_n) \\ \infty, & \text{if } z_n[k] \le \underline{z}_n \end{cases} \tag{4}$$

where $m_R > 0$ [Hz] is a design parameter that defines the mean time-to-request (MTTR). For example, if one desires a MTTR of 5 minutes when $z_n[k] \equiv Z_n^{\mathrm{set}}$ then $m_R = \frac{1}{600}$Hz. Fig. 2 shows the request probability curves for consuming and injecting packets together with the probability of remaining in stand by during coordination. The design of $\mu(z_n[k])$ for *injecting* a packet is described in similar fashion, but with boundary conditions $ii.$ above.

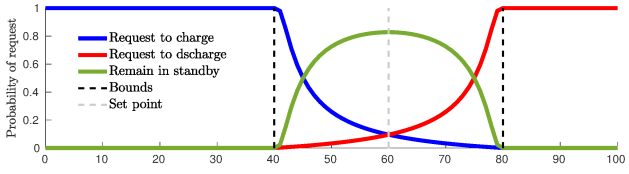

Fig. 2. Probability of request curves showing the effect of local state z_n on the packet request probabilities. The blue line corresponds to (4), the red line corresponds to packet injections (discharging packets), and the green line gives the complementary probability of remaining in standby state for a set point of 60 in the deadband [40,80] for a dynamic state z_n in arbitrary units.

Now that the dynamics of PEM are established, the VPP can produce a simple control signal that has the objective of following a reference power signal devised by an ISO grid operator. Fig. 3 shows a fleet of 100 ESSs tracking a signal with $P_{\mathrm{rate}}^{\mathrm{c}} = P_{\mathrm{rate}}^{\mathrm{d}} = 1.2$kW and the time interval is 400 minutes.

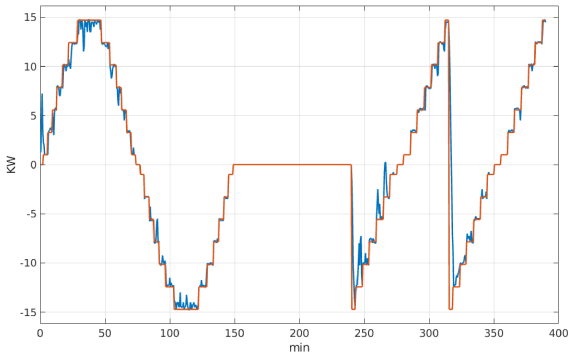

Fig. 3. A fleet of 100 ESSs under PEM tracking over an 400 minute interval consisting of a sinusoidal followed by a constant and two consecutive ramp signals.

B. Inverters under PEM

A step further for the PEM scheme implies introducing a specific grid topology. Here a linear grid model is employed, such as in prior work [2], [3], to highlight the capabilities of PEM together with a local voltage balancing control that take advantage of concurrent developments on packetized enabled power inverters [6]. For simplicity the linear grid model have been modeled with identical loads at each node in which a bidirectional ESS is interconnected with a solar PV panel and its corresponding power inverter. A diagram of the linear grid model is shown in Fig. 4. There node 0 corresponds to a substation feeder supplying a baseline voltage that is subsequently provided to N identical nodes. The resistance r_j and reactance x_j between nodes j and $j+1$ are assumed to vary maintaining the ratio $\alpha = r_j / x_j$ constant.

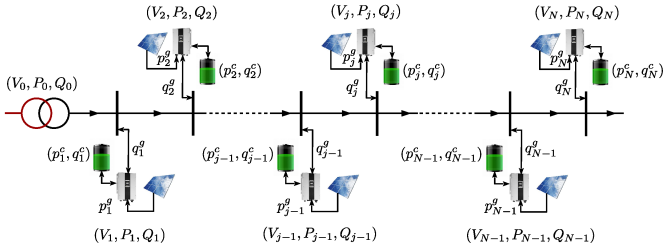

Fig. 4. Linear grid flow with packetized batteries with their corresponding solar PV and inverter configuration.

An inverter is a device that in simple words transforms direct current into alternating current. By doing this, inverters also are capable of converting active power into reactive or apparent power. This capability is what makes inverters together with PEM attractive for providing services to a grid such as voltage regulation. These devices can be enabled indirectly by the acceptance of packets which increases the amount of reactive power produced at each node. A natural setting for an inverter is at the receiving end of the power generated at a solar PV panel and then bidirectionally interacting with an ESS. For this reason, the inverter cannot control the generated power p^g but it can change its parameters so that together with the active and reactive power coming from the PEM enabled ESS generates reactive power q^I as a factor of $p^g + p^{\mathrm{d}}$, where p^{d} is the injected power

from the ESS (node load). Note here that when $p^c > 0$ then the ESS is charging (consuming power) and typically this power is all active.

An illustration of the power conversion of an inverter is given Fig. 5. Since $p^g \geq 0$, $p^d \geq 0$ when injecting, the inverter power factor conversion is limited to the first and fourth quadrants given that when $p^c > 0$ the ESS consumes power from the grid and this is done at fixed position indicated in Fig. 5. PEM can be employed to modulate how much reactive power is generated by inverters, however in this paper PEM is limited to reference tracking and the decision of accepting/rejecting packets is not influenced by how much reactive power is needed for voltage regulation. In addition, the inverters feature in this manuscript are assumed to change their power factor[1], in quadrants I and IV and in discrete steps in terms of the angle θ also illustrated in Fig. 5. To show these are realistic assumptions on inverters, a commercial-off-the-shelf (COTS) battery system provided by Enphase was shown to allow direct power factor control when discharging. Using voltage and current measurement equipment, the results of this COTS equipment characterization when requesting a variety of power factors from a single battery are given in Fig. 6, which agrees with Fig. 5. Moreover, Fig. 6 shows the range of active and reactive power that PEM enabled inverters are able to command. From collected data, the correlation between the commanded value and measured was 0.982. Also, observe that it is possible to configure the system to provide nearly only reactive power despite the fact that Enphase specifies that their AC Battery (having a built-in inverter) is controllable to a narrower range of 0.7 lead to 0.7 lag power factors.

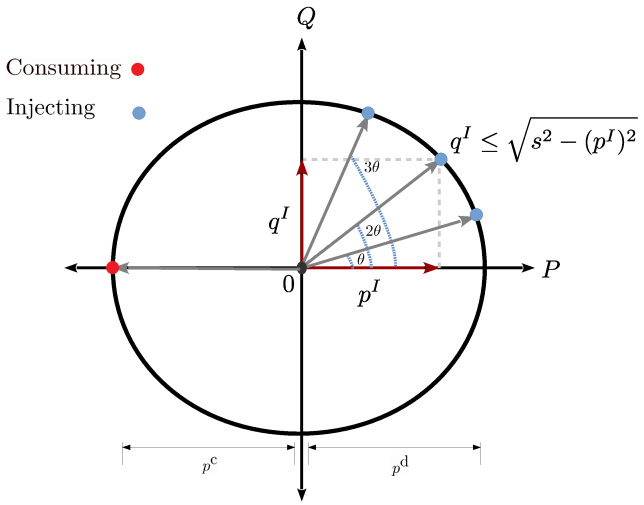

Fig. 5. Inverter reactive capability showing discrete power factor change in terms of fixed angle increments θ.

Provided that inverters and solar PV panels are connected to PEM enabled ESSs, the power flows and voltages at each node can be modeled by the following equations:

$$P_{j+1} = P_j - (p^c_{j+1} - p^g_{j+1}), \tag{5a}$$
$$Q_{j+1} = Q_j - (q^c_{j+1} - q^I_{j+1}), \tag{5b}$$
$$V_{j+1} = V_j - (r_j P_j + x_j Q_j)/V_0, \tag{5c}$$

where $P_j + iQ_j$ is the complex power flowing from node j to node $j+1$, V_j is the voltage at node j, $r_j + ix_j$ is the complex impedance between the j and $j+1$ nodes, p^c_j and q^c_j are respectively the active and reactive powers consumed at load j, and p^g_j and q^g_j are respectively the active and reactive powers generated at load j. This model and variations of it appeared in [7].

[1]Power factor here imply what percentage of p^I is transformed into q^I given the inverter size s.

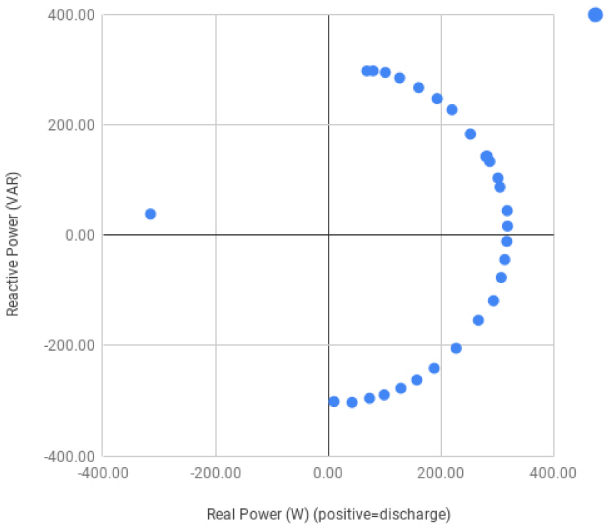

Fig. 6. Actual inverter showing the ability to control power factor from 1 to nearly 0 in the injecting side, and no ability to control power factor on the consumption side.

Note from (5a) and Fig. 5 that $p^I_j = p^c_j - p^g_j$. In the standard case, p^c_j, p^g_j and q^c_j are uncontrolled since p^g_j is generated by the PV solar panel and the other two are driven by the end-user [2], [3], [8]. However, when PEM is enabled p^c_j and q^c_j can be managed by the VPP coordinator upon the need for tracking a reference signal and given that the ESS uses the inverter as buffer between the load and the grid then PEM is used indirectly for voltage regulation.

A natural optimization objective for the linear grid resulting in (5) is to keep the losses in the power lines as small as possible. To achieve this a centralized optimization is devised by first defining the cost function

$$\mathcal{C}(P,Q,V_0,N) = \sum_{j=1}^{N-1} r_j \frac{P_j^2 + Q_j^2}{V_0^2}.$$

Then the problem is to find a solution for

$$\min_{\{q^I_j\}_{j=1,\ldots,N}} \mathcal{C}(P,Q,V_0,N) + \sum_{j=1}^{N} \left(\frac{V_j - V_0}{V_0}\right)^2$$
$$\text{s.t.} \quad 0.95 \geq V_j \leq 1.05 \text{ for all } j,$$
$$|q^I_j| \leq \sqrt{s_j^2 - (p^I_j)^2} \text{ for all } j.$$

In the majority of distribution systems the maximum allowable variation on voltage in p.u. is 0.05.

From the power flow equations (5), it can be observed that reducing the variations on voltage can be achieved by minimizing the power flow between consecutive nodes [8]. This amount to say that the absolute value of $r_j P_j + x_j Q_j$ is exactly zero whenever at every intermediate line it holds that $r_j(p^c_j - p^g_j) + x_j(q^c_j - q^I_j) = 0$, which amount to

$$q^I_j = q^c_j + \alpha(p^c_j - p^g_j). \tag{6}$$

Here it is assumed that loads at each node do not produce reactive power ($q^c_j = 0$). Furthermore, the reactive power generation of the inverters is limited by its size s_j. Thus, the local control (6) must satisfy

$$|q^I_j| \leq q^I_{j,\max} = \sqrt{s_j^2 - (p^I_j)^2}, \tag{7}$$

which is the same constraint on reactive power produced at the

inverter in the global optimization voltage regulation scheme. It should be noticed here that enabling ESSs with PEM allows one to increase the amount of reactive power that can be infused into the grid model. This indirectly leverages the packet acceptance/rejection rates into the voltage regulation problem. It is currently being investigated how is that acceptance/rejection decision can directly be used as a secondary condition for accepting packets, however that will be left as a topic of short term future research.

III. Analysis and Simulations

In this section, several simulations are presented in order to provide a glimpse of PEM actuation together with smart inverters capable of providing reactive power for voltage balancing. Here the values of p_j^g at node j have been assumed to come from a partly cloudy day where PV solar panels at all nodes form 1 to N generate $p^g = 0.2p^g_{j,\max}$ with probability 0.7 when clouds go over the panels and $p^g = p^g_{j,\max}$ with probability 0.3 otherwise. Also $p^g_{j,\max}$ is assumed to be 2kW for our scenario and the inverter size is assumed to be $s_j = 1.2p^I_{\max}$, which is reasonable given that inverters are usually oversized in relation to $p^I = p^g + p^{\mathrm{d}}$ when ESS discharge and $p^I = p^g$ when charging. The ESS loads are assumed to be ether 5kW (consuming) or -5kW (injecting). Also, the background usage for the upcoming simulations is assumed to be small $|w| << 5$kW.

A. Static scenario with PEM consumption

The first simulation provides a scenario similar to that in [2] where at a fixed point in time 100 ESSs have some consumption or injection already decided the previous instant and the inverter reacts trying to regulate voltage through the nodes under the three control laws. The first control law (global) assumes the centralized optimization approach in which a central operator has knowledge of everything that goes on at every node and therefore can control the power factor angles at which inverters provide reactive power. The result is shown in Fig. 7, where consumption (discharging) is dominant in the snapshot of time in which the simulation is computed. The latter is obvious due to the monotonically decreasing voltages.

The other cases are related to the local control law described in (6) in which the first one (local continuous) allows for q_j^I, for all j, to be any real value in $[-q^I_{j,\max}, q^I_{j,\max}]$ whereas the second one (local discrete) picks $q_j^I \in \{-q^I_{j,\max}, \ldots, -q^I_{j,i}, \ldots, 0, \ldots, q^I_{j,i}, \ldots, q^I_{j,\max}\}$ with $q^I_{j,i} = q^I_{j,\max}\sin(i\theta)$ and if $i\theta \geq 90^\circ$ then $q^I_{j,i} = q^I_{j,\max}$ as illustrated in Fig. 5. The cases for $\theta = 10^\circ, 20^\circ, 40^\circ$ and 80° are presented. Both local control laws appears to handle better the variations in voltages at the nodes as long as the θ increments are not too big. A reason why the central optimization approach does not perform better is that there is no enforcement of voltage being exactly equal to 1 and variations of it are acceptable as long as these are kept between ± 0.05 p.u. On the other hand, the discretization of the power factor in the inverter mechanics produce a deficiency of reactive power that when consuming is dominant in the grid, which results in a benefit in the performance. This was observed in the cases shown in Fig. 7 for angles 10° and 20°. This is not the case of 40° and 80° in which the discretization scheme underperformed the central optimization case.

In Fig. 7 the case where there is no reactive power control (no logic) is also shown for comparison purposes. Obviously and as expected, consumption at the nodes makes voltage to decreases and the grid deteriorates if no control action is taken. Currently, a probabilistic quantization approach is being pursued in order to capture the action of angle discretization when balancing voltage in a grid as the one described in the previous section under PEM. However, that is left for future reporting/ developments. From Fig. 7, we find that the $\theta = 20^\circ$ case provides that best performance and that value will be used in the following section to understand the dynamics associated with the proposed approach.

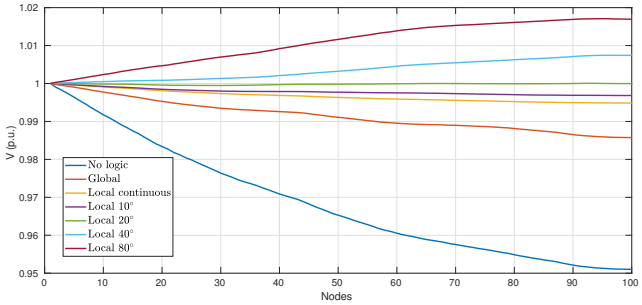

Fig. 7. Control law comparison between global, local continuous, local discretized and control where voltage is measured at the feeder (Node 0) and at 100 loads along the line.

B. Dynamic scenario with PEM consumption

The second set of simulations illustrate how PEM interact with inverters for power balancing and voltage regulation. The setting for this simulations involve a fleet of 100 ESSs with $P^{\mathrm{c}}_{\mathrm{rate}} = P^{\mathrm{d}}_{\mathrm{rate}} = 5$kW that under PEM track a reference power signal of -10kW (to incentivize ESS injections by being below the nominal response of the fleet[2]). Note that by incentivizing injections the ESS loads provide power to the inverters for its conversion into reactive power for voltage regulation at the nodes, which is the primary interest of the scheme.

Fig. 8 provides the voltage response of node 50 during tracking of the -10kW reference for the cases in which there is central optimization control (global case) and in which there is discretized PEM-based local control using angles of $\theta = 20^\circ$ steps. In general, all nodes showed better performance (voltage closer to 1 p.u.) for the local control law, and not much difference between the continuous and discretized versions of it. One expects that the larger the angle increments in the discretization scheme the more the deviation from 1 p.u. voltage. Further research is require to understand analytically the limits of the discretization scheme and it is outside the scope of this paper.

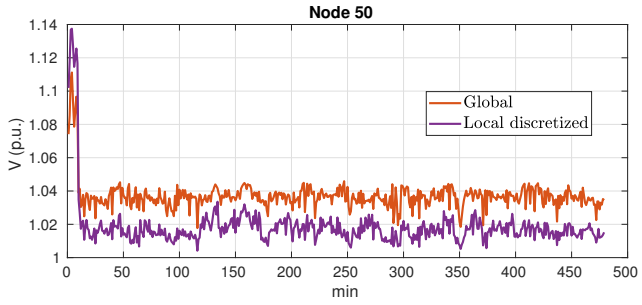

Fig. 8. PEM control law comparison with dominant consumption due to reference tracking line of -10kW for node 50.

Finally, a simple quantification of the voltage deviation is performed. First from the PEM macromodel development in [5], it is possible to assess the probability of an arbitrary ESS to be in the logic states c,sb and d. That is, when the PEM system is in steady state, which is a condition for using (5), the system dynamic can be seen as a simple Markov chain as in Fig. 9. The quantities $\beta_{\mathrm{c}}\kappa_{\mathrm{c}}, \beta_{\mathrm{d}}\kappa_{\mathrm{c}}, \beta_{\mathrm{sb,c}}, \beta_{\mathrm{sb,d}}$ represent the percentage of the population that are transitioning between states, where $\kappa_{\mathrm{c}} := P(z_{\beta_{\mathrm{c}}})$, $\kappa_{\mathrm{d}} := P(z_{\beta_{\mathrm{d}}})$ with $z_{\beta_{\mathrm{c}}}$ and $z_{\beta_{\mathrm{d}}}$ the average state of charge of the population in steady state when β_{c} and β_{d} are fixed, respectively. Also, denote by

[2]Details on the nominal response of populations under PEM can be found in [9]

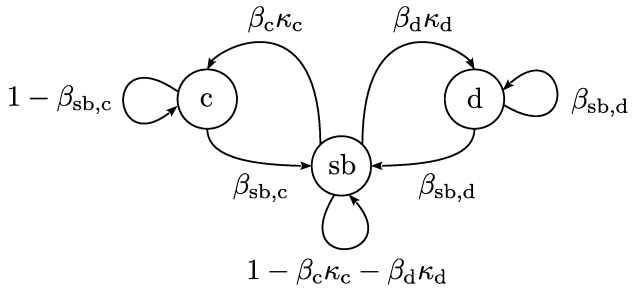

Fig. 9. Charging, discharging and standby transition in steady state.

$\pi=(\Pr(\phi=\mathrm{c}),\Pr(\phi=\mathrm{sb}),\Pr(\phi=\mathrm{d}))$ the corresponding invariant distribution of the aperiodic and irreducible Markov chain shown in Fig. 9. Now, from (5c), the voltage at a particular node, M, as a function of time can then be considered as the outcome of the summation of M random variables

$$V_M=V_0-\sum_{i=1}^{M}(r_i\widetilde{P}_i+x_i\widetilde{Q}_i),$$

where the random variables $\widetilde{P}_i:=p_i^{\mathrm{c}}-p_i^{\mathrm{g}}$ and $\widetilde{Q}_i:=-q_i^I$, where q_i^I is generated by the local control law at the inverter. Note that in steady state p_i^{c} can be treated as a random variable managed by PEM. Assuming that $P^{\mathrm{rate}}:=P^{\mathrm{rate_c}}=P^{\mathrm{rate_d}}$ for all ESSs, the index i can be drop and the random variables involved can be identified as

$$p^{\mathrm{c}}=\begin{cases} P^{\mathrm{rate}} & \text{with probability } \pi_{\mathrm{c}} \\ 0 & \text{with probability } \pi_{\mathrm{sb}} \\ -P^{\mathrm{rate}} & \text{with probability } \pi_{\mathrm{d}} \end{cases}$$

$$p^{\mathrm{g}}=\begin{cases} 0.2p^{\mathrm{g}}_{\mathrm{max}} & \text{with probability } 0.7 \\ p^{\mathrm{g}}_{\mathrm{max}} & \text{with probability } 0.3 \end{cases}$$

The mean and variances of these random variables are trivially calculated and, since they are independent of each other, they simply accumulate when these random variables are added.

It is only due to inverter sizing limiting q^I in (7) that the local law cannot make $V_i=1$ p.u. for all i. In what follows this discrepancy is quantified thanks to the fact that the probabilities of ESSs being in any of the three logic states are $\pi_{\mathrm{c}}=\Pr(\phi=\mathrm{c}),\pi_{\mathrm{sb}}=\Pr(\phi=\mathrm{sb})$ and $\pi_{\mathrm{d}}=\Pr(\phi=\mathrm{d})$. As mentioned previously, the values for $\kappa_{\mathrm{c}},\kappa_{\mathrm{sb}}$ and κ_{d} in the Markov chain in Fig. 9 are obtained as a function of the probability of request function in (3) and the percentages of acceptance and rejection of packets corresponding to the desired state of charge level of the average ESS. The expected deviation from 1 p.u. at node M in relation to node $M-1$ is then

$$\begin{aligned} V_M-V_{M-1}=&r_M(E[p^{\mathrm{c}}]-E[p^{\mathrm{g}}]) \\ &-x_M\min\left\{\alpha(E[p^{\mathrm{c}}]-E[p^{\mathrm{g}}]),E\left[\sqrt{s^2-(p^I)^2}\right]\right\}, \end{aligned}$$

where $p^I=p^{\mathrm{rate}}+p^{\mathrm{g}}$ with probability π_{d} and p^{g} with probability $1-\pi_{\mathrm{d}}$ given that inverters can only provide reactive power from the ESSs when they are injecting power. When $\alpha(E[p^{\mathrm{c}}]-E[p^{\mathrm{g}}])<E\left[\sqrt{s^2-(p^I)^2}\right]$ at node M, a bound for the variation in voltage is

$$V_M-V_{M-1}<r_M(E[p^{\mathrm{c}}]-E[p^{\mathrm{g}}])-x_ME\left[\sqrt{s^2-(p^I)^2}\right]. \quad (8)$$

Defining $\Delta V_N=\max_{M=1,\ldots,N}\{V_M-V_{M-1}$ s.t. right hand side of (8) is positive$\}$ and since V_M-V_{M-1} occurs independently at each node, the deviation of voltage at node M from 1 p.u. is bounded as

$$|V_M-1|<R\Delta V_N,$$

where R is the average number of nodes before node M for which the right hand side of (8) is positive. In Fig. 8, the resulting bound for node 50 is $|V_{50}-1|<0.056$ p.u. for $R\approx 28$ and the actual mean value of the voltage at the same node is 0.033 p.u. Due to space limitations further analysis of the bounds that includes computing its standard deviation is deferred for a future publication.

IV. Conclusions and Future Work

The work herein showed that asynchronous and distributed coordination of distributed battery resources can be used to maintain desired line voltage on a feeder. Specifically, battery systems being coordinated through a packetized energy management strategy autonomously adjusted their inverter's power factor when injecting power. Through simulations it was illustrated how this decentralized approach performed better than a centralized approach. In addition, a simple bound for the voltage deviation at each know was provided.

Future work will be to adapt this work so that inverter operations are compliant with the IEEE 1547 standard [10]. In addition, development for inverter sizing design is ongoing.

Acknowledgement

The authors would like to thank the technical staff at Enphase for providing the assistance that enabled our team to implement PEM on their systems and the team at Packetized Energy for performing the hardware testing.

References

[1] Deloitte Center for Energy Solutions, "Managing variable and distributed energy resources: A new era for the grid." Deloitte Development LLC, 2016.

[2] S. Kundu, S. Backhaus, and I. A. Hiskens, "Distributed control of reactive power from photovoltaic inverters," in *2013 IEEE International Symposium on Circuits and Systems (ISCAS2013)*, May 2013, pp. 249–252.

[3] K. Turitsyn, P. Šulc, S. Backhaus, and M. Chertkov, "Distributed control of reactive power flow in a radial distribution circuit with high photovoltaic penetration," in *IEEE PES General Meeting*, July 2010, pp. 1–6.

[4] M. Almassalkhi, J. Frolik, and P. Hines, "Packetized energy management: Asynchronous and anonymous coordination of thermostatically controlled loads," in *2017 American Control Conference*, May 2017, pp. 1431–1437.

[5] L. A. Duffaut Espinosa, M. Almassalkhi, P. Hines, and J. Frolik, "Aggregate modeling and coordination of diverse energy resources under packetized energy management," in *56th IEEE Conference on Decision and Control*, December 2017, pp. 1394–1400.

[6] A. Giroux, F. Wallace, J. Frolik, and L. A. Duffaut Espinosa, "Coordination of distributed battery systems using packetized energy management," in *10th Conference on Innovative Smart Grid Technologies*, 2019, under review.

[7] M. Baran and F. F. Wu, "Optimal sizing of capacitors placed on a radial distribution system," *IEEE Transactions on Power Delivery*, vol. 4, no. 1, pp. 735–743, Jan 1989.

[8] K. Turitsyn, P. Šulc, S. Backhaus, and M. Chertkov, "Local control of reactive power by distributed photovoltaic generators," in *2010 First IEEE International Conference on Smart Grid Communications*, Oct 2010, pp. 79–84.

[9] L. A. Duffaut Espinosa, M. Almassalkhi, P. Hines, and J. Frolik, "System properties of packetized energy management for aggregated diverse resources," *Power Systems Computation Conference*, June 2018.

[10] IEEE Standards Coordinating Committee 21, "IEEE Standard for Interconnection and Interoperability of Distributed Energy Resources with Associated Electric Power Systems Interfaces." IEEE, 2018.